An a priori DNS subgrid analysis of the presumed β-PDF model

INTERNATIONAL JOURNAL OF HYDROGEN ENERGY 40 (2015) 12811–12823

Available online at www.sciencedirect.com

ScienceDirect

journal homepage: www.elsevier.com/locate/he

An *a priori* DNS subgrid analysis of the presumed β-PDF model

A. Donini [a,*], R.J.M. Bastiaans [a], J.A. van Oijen [a], M.S. Day [b], L.P.H. de Goey [a]

[a] Combustion Technology Group, Department of Mechanical Engineering, Eindhoven University of Technology, De Rondom 70, 5612 AP Eindhoven, The Netherlands

[b] Lawrence Berkeley National Lab, 1 Cyclotron Rd., Berkeley, CA 94720, USA

ARTICLE INFO

Article history:
Received 29 April 2015
Received in revised form
21 July 2015
Accepted 23 July 2015
Available online 15 August 2015

Keywords:
Beta-pdf
Presumed
Hydrogen
Turbulent
Subgrid
Premixed

ABSTRACT

A common way of carrying out LES or RANS of premixed and partially premixed turbulent flames with tabulated combustion chemistry consists of using a presumed shape for the probability density function (PDF) of progress variable and mixture fraction in order to compute the reaction rates. Commonly utilized for this purpose is the β-function PDF. To the aim of clarifying the applicability of the presumed β-PDF approach to the modeling of methane and hydrogen turbulent premixed flames, in this paper an investigation of the probability density distribution is performed by processing three-dimensional DNS computational results performed with detailed chemistry. This analysis is performed by means of a detailed comparison between the DNS data and the corresponding *a priori* LES obtained with top-hat filters of various sizes. The analysis is conducted for hydrogen and methane turbulent flames, for comparison. In particular, it is assessed whether a lean premixed turbulent hydrogen-air flame can be well-represented in LES by a β-PDF approach as traditionally applied for methane in literature. It is shown that the presumed β-PDF model performs rather well for both hydrogen and methane. The total error between the real distribution and the presumed β-PDF is of comparable amount for the two fuels. However, the error shows a more consistent profile in methane flames. In addition, it is shown that mean and variance are not sufficient as control parameters for an improved modeling of hydrogen flames by means of presumed PDF, plausibly because of its strong differentially diffusive effects.

Introduction

In industry the development of clean and efficient technologies for the combustion process is achieved by a combination of experimental and numerical research. Physical testing is in general extremely expensive and time consuming as well, whereas modern engineering trends tend towards shorter and more efficient design cycles. A great reduction of the costs could be made by maximizing the usage of simulations in the design phase. These reasons, together with the persisting

* *Corresponding author.*
E-mail address: andrea.donini@gmail.com (A. Donini).
http://dx.doi.org/10.1016/j.ijhydene.2015.07.110

advance in the computer technology, are sufficient to elucidate the phenomenal growth of interest in Computational Fluid Dynamics (CFD) of reacting flows in the last few decades.

Nevertheless, the numerical modeling of combustion systems still represents a remarkably challenging task. The interaction of turbulence, chemical reactions and thermodynamics in reacting flows is of exceptional complexity. In addition to this, modern lean-premixed highly turbulent combustion is inherently unstable, requiring therefore additional effort in the modeling. This especially applies if considering the combustion of alternative fuels, such as hydrogen. This problem is overcome by the introduction of a form of averaging in the governing equations, which reduces the computational cost. Nonetheless, averaging involves loss of information, with the result that the number of unknowns always exceeds the number of equations. Appropriate models are therefore essential in order to solve the governing physics. Large-Eddy Simulation (LES) and Reynolds-averaged Navier–Stokes (RANS) methods reduce the computational cost of the flow simulation by filtering the flow solution either in space or in time. Combustion models aim to reduce the aforementioned computational of flame simulations mainly by a reduction of the number of equations which need to be solved for the reaction, without significantly compromising the quality of results. The combination of these strategies give rise to unknown sub-filter contributions for both flow and combustion chemistry, which need to be modeled concurrently.

A standard way of carrying out LES or RANS with tabulated combustion chemistry e.g. like FGM [1,2] or FPI [3] is to use a presumed shape for the probability density function (PDF) of progress variable and mixture fraction to compute reaction rates in premixed and partially premixed turbulent flames. In this method, a variable is described locally by a presumed-shape PDF defining the probability of occurrence of a certain state. Commonly utilized for this purpose is the β-function PDF, which was proposed by Ref. [4] in the non-premixed framework, and since then it has become a standard closure technique for premixed and partially premixed flames [5–11]. Although the choice of any of this particular PDF shapes appears to be totally arbitrary as far as the inherent physics of turbulent combustion is concerned, the presumed β-PDF model provides a plausible (although not exact) description of chemistry sub-grid terms [8]. The β-PDF is defined on the continuum between 0 and 1, and it is very versatile whereas it is determined by two parameters (the value of the first and second moment, i.e. mean and variance) solely. Moreover, this function is able to take a wide variety of different shapes (among the symmetric, uniform and bi-modal) as shown in Fig. 1, including integrable singularities near the end points.

Successful validation of the method has been obtained for diffusion flames. On the other hand, to the best of the authors knowledge, the β-function shape for the presumed PDF has never been endorsed by basic physical arguments in the framework of premixed turbulent combustion. Simplicity of implementation and numerical efficiency are the main reasons for its wide utilization. Despite the fact that such reasons are of undeniable importance, the use of β-function PDF does not seem to be a genuine approach until this is justified by fundamental arguments or by comprehensive DNS

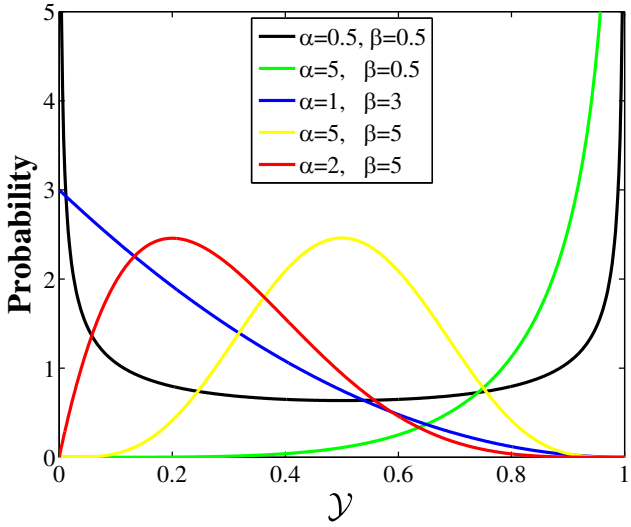

Fig. 1 – Probability density function shapes for the β-distribution with different parameters.

experimental studies. Studies analyzed the β-PDF behavior in premixed flames by evaluating actual distributions [12], nonetheless considering homogeneous slices of the whole domain and therefore neglecting local effects. Local effects are especially important in the combustion of fuel which are characterized by a marked differential diffusion, such as hydrogen flames, as further described in the following sections.

To the aim of clarifying the applicability of the presumed β-PDF approach to the modeling of methane and hydrogen turbulent premixed flames, an investigation of the probability density distribution is performed by processing three-dimensional DNS computational results performed with detailed chemistry [13,14]. To have an *a priori* quantitative comparison of the effectiveness of the prediction given by this model it is useful to compare it locally with the real probability distribution, calculating therefore the affinity between the two distributions in a point to point fashion. In order to do so, the paper is structured as follows: first in Section 2 the properties of the β-PDF are recalled, then in Section 3 the data used for the analysis is introduced and described. Thereafter the results of this analysis are presented and interpreted in Section 4, finalized by the concluding remarks of Section 5.

The β-function PDF distribution

In probability theory, a probability density function (PDF) of a variable $\mathcal{X} \in (a, b)$ is a function that describes the relative likelihood for this random variable to take on a given value. The probability density function is non-negative

$$P(\mathcal{X}) \geq 0, \tag{1}$$

and it satisfies the normalization condition:

$$\int_a^b P(\mathcal{X}) d\mathcal{X} = 1. \tag{2}$$

The definition of the β-function PDF for the reaction progress variable $\mathcal{Y}$ (defined on the continuum between $0 \leq \mathcal{Y} \leq 1$) is:

$$P(\mathcal{Y}) = \frac{\Gamma(\alpha+\beta)}{\Gamma(\alpha)\Gamma(\beta)}\mathcal{Y}^{\alpha-1}(1-\mathcal{Y})^{\beta-1}, \quad (3)$$

where $P(\mathcal{Y})$ is the probability distribution and Γ is the gamma function, which can be calculated efficiently with a fifth-order polynomial approximation [15]. The two parameters α and β are given by:

$$\alpha = \overline{\mathcal{Y}}\left(\frac{\overline{\mathcal{Y}}(1-\overline{\mathcal{Y}})}{var(\mathcal{Y})} - 1\right), \quad (4)$$

$$\beta = \left(\frac{\alpha}{\overline{\mathcal{Y}}}\right) - \alpha. \quad (5)$$

This function is based on the first two moments of $\mathcal{Y}$: the mean $\overline{\mathcal{Y}}$ and the variance $var(\mathcal{Y})$. As mentioned earlier, this presumed form provides a flexible range of shapes, as shown in Fig. 1. If α and β approach zero (large variance) the PDF assumes a bi-modal shape. On the contrary, when α and β are large the PDF assumes a mono-modal shape with an internal peak. In the case that the variance is very small the PDF behaves like a Gaussian instead. Nonetheless, it should be noted that not every shape which may occur in premixed flames can be reproduced by the β-function PDF. In the case that $\alpha < 1$ (or $\beta < 1$) the PDF tends to infinity and resembles a Dirac delta function at $\mathcal{Y} \to 0$ (or respectively at $\mathcal{Y} \to 1$). However, contrary to the Dirac delta function, if both $\overline{\mathcal{Y}} \ll 1$ and $\alpha \ll 1$ (large variance) the probability of finding unburned mixture vanishes. Similarly, the probability of finding burned mixture also becomes zero if $\overline{\mathcal{Y}} \gg 0$ and $\beta \ll 1$. In addition, the β-function PDF is not capable to reproduce a double peak shape, as one would expect in the combustion of highly diffusive fuels. These drawbacks of the approach should be taken into account when considering the presumed β-function PDF model.

Description of the DNS data

The three-dimensional DNS data-sets analyzed in this paper represent premixed turbulent flames in a statistically one-dimensional configuration. Two different fuels are investigated: hydrogen and methane. Turbulence-flame interactions for these cases are characterized using effective *Ka* and *Da* definitions, as described in Ref. [16]. Specifically, turbulence intensity and length scales are normalized to the propagation speed and thermal thickness of comparable flames in the absence of turbulent fluctuations (i.e. freely propagating premixed flames). In that setting, the low Lewis number hydrogen case tends to spontaneously form highly curved cellular (nonuniform) burning patterns. Globally, such flames tend to burn with an enhanced mean propagation speed and with decreased thermal thickness, relative to the comparable 1D steady unstrained flame at a comparable mixture. Unity Lewis number fuels, such as the lean methane mixture here, are not susceptible to these instabilities, and have a local structure that is well-approximated by the idealized model. It was shown [16,14] that Ka_{eff} and Da_{eff}, based on the structure of the freely propagating flames, lead to characterizations of turbulence–chemistry interactions that are independent of Lewis number.

The simulations are based on a low Mach number numerical formulation of the reacting flow equations [13,17]. A mixture-averaged model for species diffusion is used and the transport coefficients, thermodynamic relationships and chemical kinetics are obtained from the Gri-Mech 2.11 chemical reaction mechanism [18]. The integration algorithm has an adaptive local grid refinement [19] and it is second order accurate in space and time.

The configuration consists of a rectangular domain with a square cross-section of side L, and a height of $8L$, oriented such that the flame propagates downward. The hot combustion products flow freely out of the top of the domain, whereas the bottom boundary is an adiabatic free slip wall. The lateral boundaries are periodic. A flat freely propagating flame is initialized at the top, while the premixed cold fuel mixture ($T_u = 298$ K) is specified at the square bottom boundary. The simulations are performed on a base grid of $256 \times 256 \times 2048$ uniform cells, with two levels of factor-of-two mesh refinement that dynamically track regions of high chemical reactivity and vorticity as the flame evolves in a quasi-steady configuration. The effective grid size results in $1024 \times 1024 \times 8192$ points. For further details on the simulations and numerical methods please refer to [12,16,13,17].

The two cases subject to the analysis are specified in Table 1. Here, ϕ is the equivalence ratio, L is the side size, δ_L^0 the laminar flame thickness, δ_r the inner layer thickness, Ka the Karlovitz number, Da the Damköhler number and $\mathcal{L}$ the integral scale.

Effective Karlovitz and Damköhler numbers are given for the hydrogen case.

Representative snapshots of the solution for the hydrogen and methane flames are shown in Figs. 2 and 3, respectively, where temperature, density and fuel consumption rate are plotted on a vertical slice plane at the center of the domain. It is clearly noticeable for the hydrogen case how thermo-diffusive instabilities (i.e. differential diffusion effects) lead to the breakdown of the flat laminar flame sheet, resulting in a cellular burning structure (this effect is noticeable from super-adiabatic temperatures and non-uniform temperature at the outlet, which are due to local variations of mixture fraction).

The effects of differential diffusion on the flame properties may be described for instance by comparison with one-

Table 1 – Description of the analyzed cases.

	Hydrogen	Methane
ϕ	0.4	0.7
L [m]	0.0164	0.0264
δ_L^0 [m]	6.82×10^{-4}	6.6×10^{-4}
δ_r [m]	1.3×10^{-5}	2.28×10^{-5}
Ka	47.7	12.0
Da	0.14	0.481
Ka_{eff}	12.0	12.0
Da_{eff}	0.481	0.481
$\mathcal{L}$ [m]	0.00164	0.00264
u RMS	3.948	1.570
Grid Resolution [m]	16×10^{-6}	25.8×10^{-6}

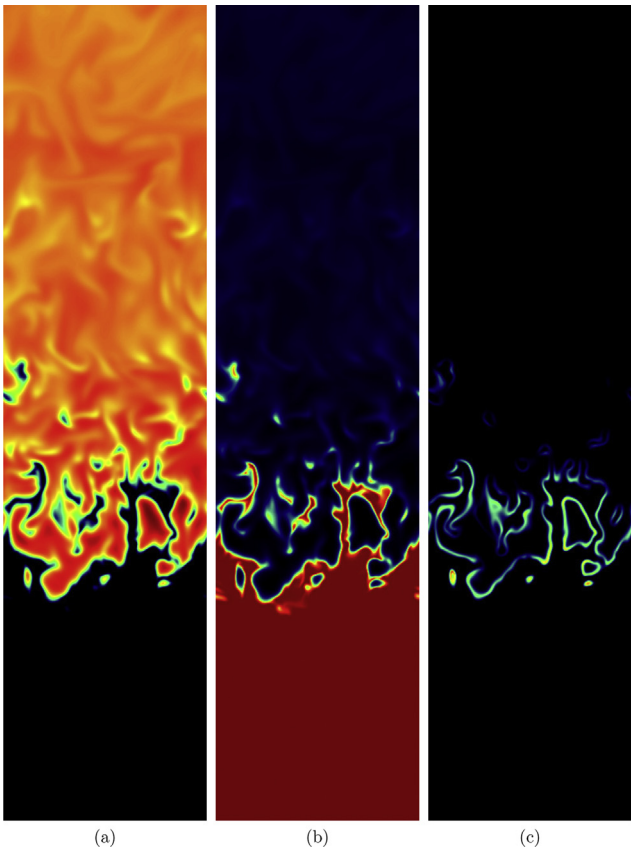

Fig. 2 – Hydrogen case: solution plots on a slice plane. (a) Temperature, with range 298–1770 [K]. (b) Density, with range 0.178–1.033 [kg m^{-3}]. (c) Hydrogen consumption rate, with range 0–90 [kg m^{-3} s^{-1}].

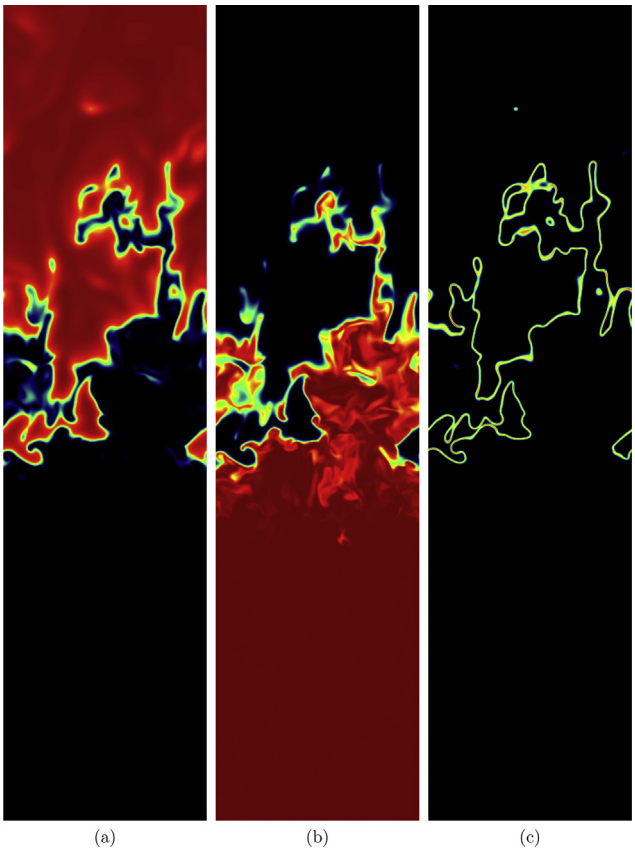

Fig. 3 – Methane case: solution plots on a slice plane. (a) Temperature, with range 298–1870 [K]. (b) Density, with range 0.183–1.144 [kg m^{-3}]. (c) Methane consumption rate, with range 0–62 [kg m^{-3} s^{-1}].

dimensional simulations. To this purpose, laminar free adiabatic premixed flames are computed with detailed chemistry at the same conditions of the 3-D data, both with mixture averaged transport (i.e. non-constant Lewis number) and unity Lewis number. The flames are computed with the specialized 1D flame code Chem1D [20]. Table 2 delineates a list of properties evaluated on the basis of the resulting one-dimensional flames. The influence of differential diffusion is clearly visible on the burning velocity and mass burning rate, particularly for hydrogen which in fact has a very low Lewis number. This is due to the varying distribution of enthalpy (and mixture fraction) along the flame. Note that enthalpy is conserved in the complete domain. An analogous type of investigation can be done observing the peaks of temperature on the basis of the one-dimensional data and three-dimensional results. The outcome of this comparison is shown in Table 3. The temperature peaks of the 3D data are considerably higher than in the 1D case, with a substantial 346 K difference for the highly diffusive hydrogen flame. The methane flame temperature is hardly changed since Le $\approx$ 1. A similar effect can be noticed from the OH mass fraction and heat release maximum values, which represent a valuable indication of the strength of the reaction. This displays once more a difference for the methane case and an extensive difference for the hydrogen case. Considering the presence of the above mentioned strong differential diffusion effects, it is of great significance to observe how the presumed β-shaped PDF behaves in such conditions.

The *a priori* subgrid analysis

Aim of this analysis is to have a local sub-grid scale assessment of the analogy between β-PDF and the computed real probability distribution. To this aim, an *a priori* quantitative comparison is performed on the DNS data described in Section 3, in a point to point fashion. The numerical procedure to achieve such a comparison proceeds as follows.

- For every grid point in the domain a "sub-box" of surrounding points is built to emulate a LES filter sub-box with predefined dimension.
- The probability density distribution of the progress variable is evaluated inside the sub-box.
- The mean and variance of the progress variable are evaluated inside the sub-box. This operation is equivalent to using a top-hat filter with size of the sub-box. These two values are then used to calculate the β-distribution inside the local sub-volume.

Table 2 – One dimensional flat flame results. Differential diffusion effects on a series of flame parameters.

	H_2	H_2 Le = 1	CH_4	CH_4 Le = 1
Enthalpy @ inlet/outlet [J kg^{-1}]	−135.9	−135.9	-1.827×10^5	-1.827×10^5
Maximum Enthalpy [J kg^{-1}]	932.7	−135.9	-1.167×10^5	-1.827×10^5
Minimum Enthalpy [J kg^{-1}]	-5.439×10^4	−135.9	-1.988×10^5	-1.827×10^5
Mass Burning Rate [kg m^{-2} s^{-1}]	0.163	0.351	0.211	0.216
Burning Velocity [m s^{-1}]	0.159	0.344	0.185	0.189

- The two distributions are compared by calculating an error between them.
- This procedure is repeated for every point in the domain.

The progress variable represents the evolution of the combustion process from unburned to burned, and it is defined by the fuel mass fraction (i.e. hydrogen or methane according to the case under consideration). The real distribution inside every sub-volume is computed through a discrete binning procedure. The number of bins in which the local progress variable range is divided is equal to three times the number of points of the side of the sub-box N. Therefore, a box of N × N × N grid points makes use of 3N bins in the $\mathcal{Y}$ space. This choice is made in order to have a minimum number of empty bins. This procedure allows to effectively perform a detailed comparison between the DNS data and the corresponding *a priori* LES obtained with a top-hat filter.

Figs. 4 and 5 show examples of distributions collected on randomly chosen sub-boxes that span the flame surface for the hydrogen and methane cases, respectively, for a range of sub-box sizes. For each point a surrounding sub-volume is defined, and the real and the calculated β-distribution are shown together. These examples are quite important in order to capture qualitatively the accordance of the two distributions. In this figure the size of the cubic sub-volume is expressed by its side length. The size of the box increases from top to bottom figure, while the averaged progress variable increases from left to right figure.

As previously pointed out, the β-function is calculated with mean and variance of the progress variable of the local sub-volume. In the same manner, the minimum and maximum values of progress variable (fuel mass fraction) are set locally in each sub-volume. However, differential diffusion effects lead to a varying distribution of heat and mixture fraction along the flame, generating zones in which the local enthalpy and equivalence ratio differ from the inlet conditions (this effect is shown for the same configuration in the JPDFs of [21]). Therefore, the definition of a global progress variable must take into account these extended limits, which are not known *a priori*. Choosing to define the progress variable on the basis of the local extents means excluding the issue of defining it globally. It is to note that this choice introduces some limitations on the investigation here presented, as discussed in the concluding remarks of this section.

In order to define the disagreement between the assumed and real PDF quantitatively, a representative measure must be taken into account. A normalized error between β-PDF and the real probability distribution inside a single sub-volume can be defined as follows:

$$e = \frac{\int_0^1 \left| P(\mathcal{Y})_\beta - P(\mathcal{Y})_{DNS} \right| d\mathcal{Y}}{e_{nn,max}}, \tag{6}$$

where the subscript DNS indicates the real values of the PDF, while β is the presumed β-PDF calculated from the actual mean and variance evaluated in the sub-box. This error is normalized in order to have it ranging between 0 (perfect agreement between the two PDFs) and 1 (the two PDFs are completely non correlated). The coefficient $e_{nn,max}$ is the maximum non-normalized error. The value of $e_{nn,max}$ is easily calculated given the normalization condition of Equation (2). The error as defined in Equation (6) is merely an area subtraction, as shown schematically in Fig. 6a. The maximum error is given by two completely uncorrelated PDFs, e.g. in the case of Fig. 6b. Taking into account Equation (2), for this last case it results $e_{nn,max} = 2$.

Since the DNS PDF is calculated in a discrete form, the error needs to be written in a discrete form as well. The domain of the PDF, going from 0 to 1, is therefore divided into a discrete number of elements (bins). Supposing that the β-PDF is discretized on the same elements as the DNS sub-grid PDF, the error inside a single sub-volume is given by

$$e = \frac{\sum_1^{N_{bins}} \left| P(\mathcal{Y})_{i,\beta} - P(\mathcal{Y})_{i,DNS} \right| \Delta\mathcal{Y}}{e_{nn,max}} \tag{7}$$

where N_{bins} is the number of bins of the real distribution and P_i is the value of the probability of bin i.

Another important factor to take into consideration in the analysis is the impact that such an error would lead to the representation of the modeled source terms.

Table 3 – One-dimensional flat flame results compared with three-dimensional data. Differential diffusion effects on the maximum flame temperature and OH mass fractions.

	H_2 1-D	H_2 3-D	CH_4 1-D	CH_4 3-D
Max. Temperature [K]	1426.2	1772.3	1842.1	1863.4
Maximum Y_{OH}	9.25×10^{-4}	64.01×10^{-4}	2.43×10^{-3}	2.89×10^{-3}
Max. Heat Release [W m^{-3}]	4.46×10^8	6.28×10^9	1.35×10^9	1.94×10^9

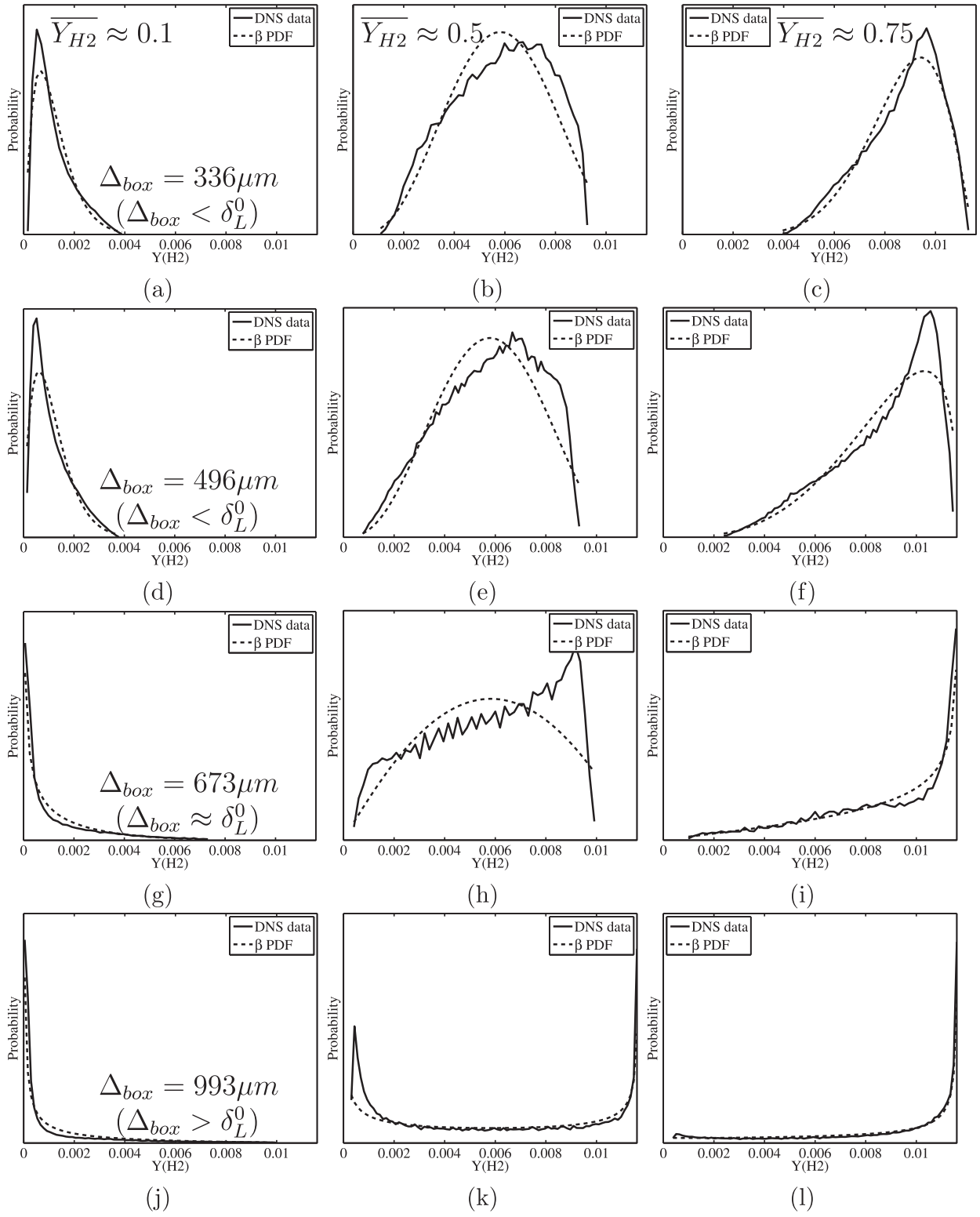

Fig. 4 – Hydrogen case. Comparison of the real probability distribution and corresponding β-distribution in randomly chosen sub-volumes. Equal sub-volume sizes (Δ_{box}) are shown on the same row of figures, while columns are for similar mean value of the fuel mass fraction inside the sub-volume ($\overline{Y_{H2}}$). The number of grid points on the cubic sub-volume side are: (a,b,c) 21, (d,e,f) 31, (g,h,i) 42, (j,k,l) 62.

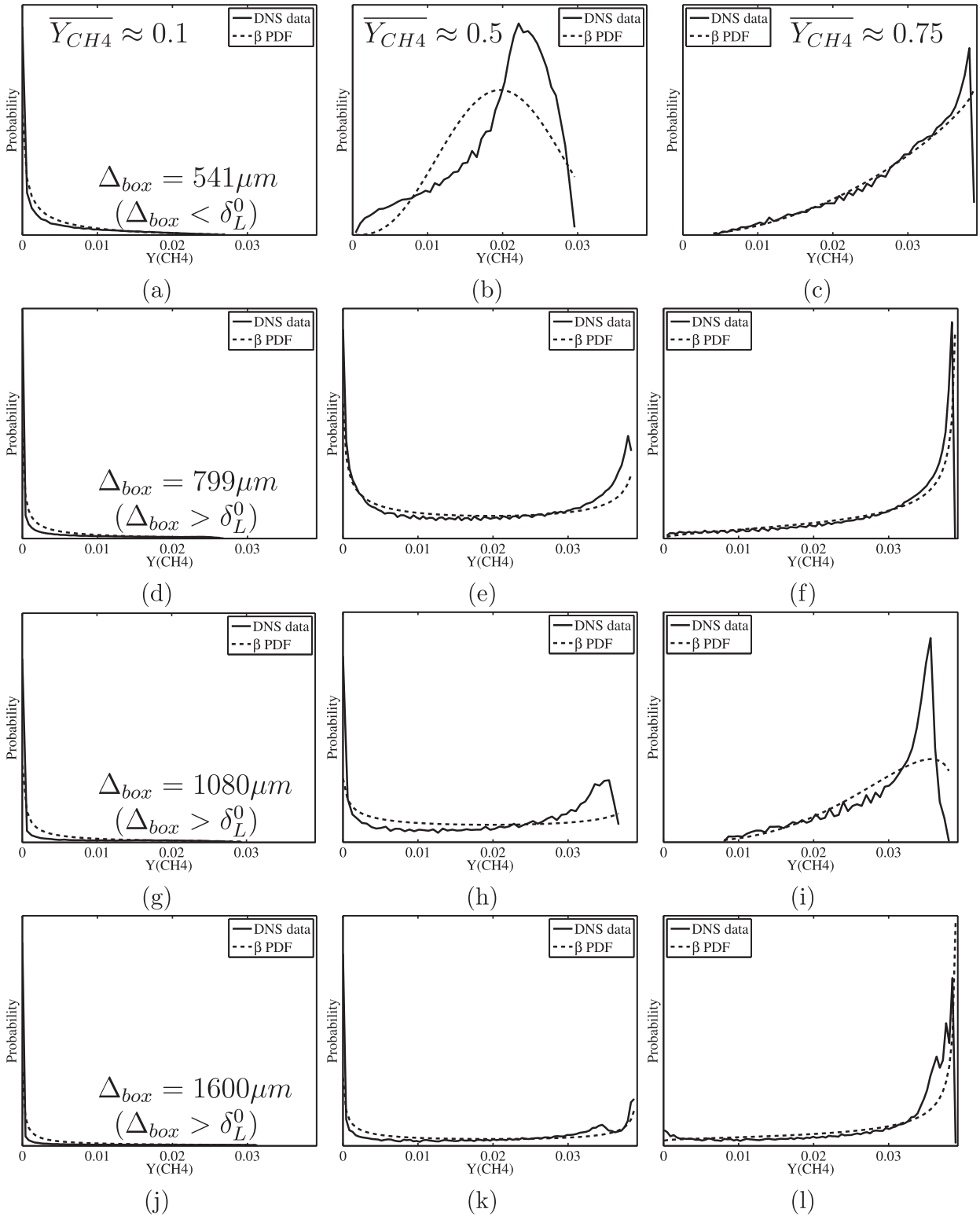

Fig. 5 – Methane case. Comparison of the real probability distribution and corresponding β-distribution in randomly chosen sub-volumes. Equal sub-volume sizes (Δ_{box}) are shown on the same row of figures, while columns are for similar mean value of the fuel mass fraction inside the sub-volume ($\overline{Y_{CH4}}$). The number of grid points on the cubic sub-volume side are: (a,b,c) 21, (d,e,f) 31, (g,h,i) 42, (j,k,l) 62.

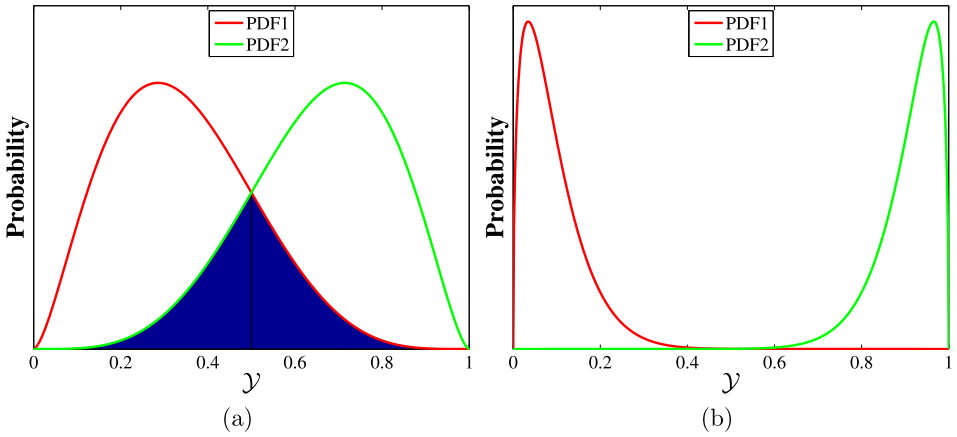

Fig. 6 – Schematical representation of the mutual area of two PDFs. (a) The blue area is common between the two PDFs. (b) Completely uncorrelated PDFs. (For interpretation of the references to color in this figure legend, the reader is referred to the web version of this article.)

As a result of this procedure an error value is obtained for each point in the domain. Joint PDF of the error between the real distribution and the corresponding β-PDF as a function of the (normalized) fuel mass fraction are shown for different sub-volume sizes in Figs. 7 and 8, for hydrogen and methane. The colors range from blue (zero error probability) to red (maximum error probability). A large clustering of points is present at the edges of the domain, where the fresh and exhaust mixture is located. This feature is due to the fact that the active flame region occupies a minor volume in the domain.

As a general observation, the presumed β-PDF gives rather good results, in terms of overall error. This is valid for both fuels, which is somewhat different from what previously observed in literature. The largest part of the error between real and presumed distribution is observed close to the burned and unburned regions. A distinction of zones of interest can be made along the flame region, e.g. by dividing the progress variable (i.e. the fuel mass fraction) interval in three sections: the region close to the burned mixture $0 \leq Y_{fuel,norm} < 0.4$, the central flame zone $0.4 \leq Y_{fuel,norm} < 0.6$ and the region close to the fresh mixture $0.6 \leq Y_{fuel,norm} \leq 1$. A general distinction between the error distribution in these three regions can be observed. Rather scattered error values are found close to the unburned side, especially in the hydrogen case which shows a very low coherency. Dissimilarly, in the proximity of zero fuel mass fraction the error shows a more compact and marked trend, and this feature is especially notable for the methane case. Such a type of behavior can be interpreted as a systematic error. In this sense, this leads to the conclusion that the presumed β-PDF model could be improved for methane combustion e.g. by adopting a different PDF shape (or introducing an ad hoc empirical tuning of the β-PDF shape), whereas still keeping the advantage of being simply determined by the two parameters mean and variance. The central flame regions are the ones in which the presumed β-PDF model performs best. This is a positive feature, in fact an accurate modeling of this region of the flame is of great importance in premixed flames, since it typically features highly non-linear variations of source terms.

As a general observation, the error distribution for the hydrogen case is rather scattered, and does not present any dominant coherence. Such evidence effectively demonstrates that mean and variance are not sufficient as control parameters for an accurate modeling of hydrogen flames by means of presumed PDF. This fact is opposed to what is formerly determined for methane, for which the first two moments seem to deliver fairly coherent results. Differential diffusion (leading to varying distribution of enthalpy and mixture fraction along the flame) is the plausible cause for this difference, and a legitimate presumed PDF for hydrogen simulations should include extra controlling parameters to describe such phenomena.

This can be considered by visualizing the source term distribution along the flame. This is given in Fig. 9, in which 1D premixed flames computation results are shown (at the same conditions of the 3D turbulent flame under investigation). The figure represents the fuel consumption term versus its mass fraction, for the two different fuels, normalized by their extreme values. From this figure it is clear how the source term distribution is quite different for the two different fuels. Methane source term is more spread along the flame, making this type of flame more sensitive to an incorrect modeling of the initial and central part of the flame.

The results of error distribution as shown in Figs. 7 and 8 give interesting insights on the presumed β-PDF performance. However these do not give sufficient quantitative indications on the error. For this purpose, it is useful to calculate the overall error, and assess the character of its dependence on the sub-grid size in order to compare the overall value and trends. Fig. 10a and b display the averaged (over the whole domain) values of the normalized error as a function of the sub-volume size, respectively for the hydrogen and methane case. For both cases the error level is rather similar, which is somewhat different from what observed in Ref. [12]. Nonetheless, local effects are neglected

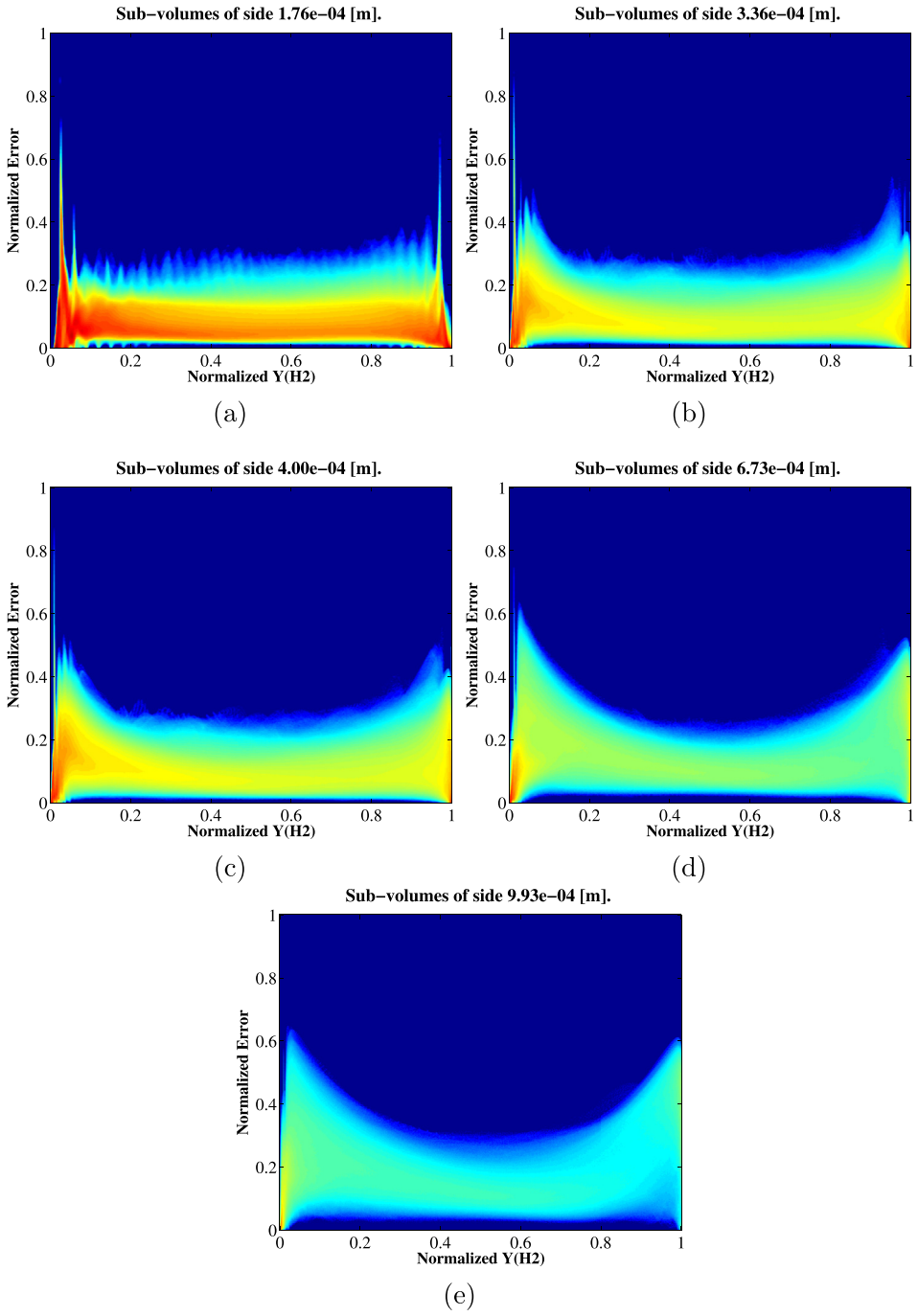

Fig. 7 – Hydrogen case. Joint PDF of the error (between the real and β-distribution) and the normalized mean fuel mass fraction for different sub-volume sizes. The colors range from blue to red, which are respectively the minimum and maximum error probability of each figure. The number of grid points on the cubic sub-volume side are: (a) 11, (b) 21, (c) 25, (d) 42, (e) 62. (For interpretation of the references to color in this figure legend, the reader is referred to the web version of this article.)

in Ref. [12] where homogeneous slices of the whole domain are considered, which is a very different approach with respect to the one adopted in the present work. It is interesting to note that for both fuels the error increases for increasing volume size. This is typically expected, since a bigger sub-volume implies more non-linearities to be modeled. However, it is very interesting to note that the error slope is linear (i.e. linearly increasing with the sub-volume side length, not the volume). This is due to the fact that the turbulent flame is an aggregate of thin locally one-dimensional flamelet structures, and therefore the error is locally distributed one-dimensionally. Furthermore, a minimum appears to exist for both cases. However for hydrogen itself this shows a more pronounced nature. This is most

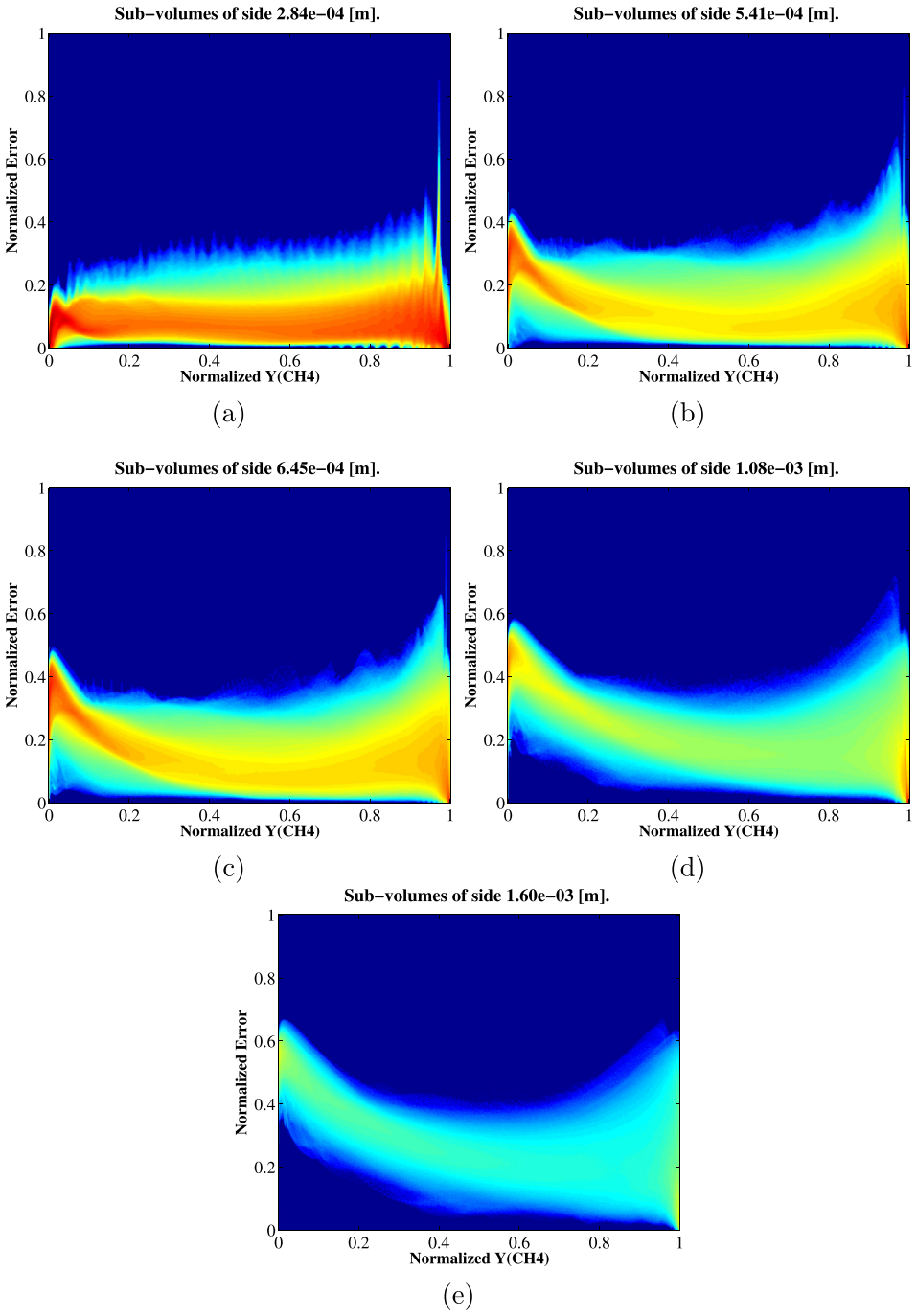

Fig. 8 – Methane case. Joint PDF of the error (between the real and β-distribution) and the normalized mean fuel mass fraction for different sub-volume sizes. The colors range from blue to red, which are respectively the minimum and maximum error probability of each figure. The number of grid points on the cubic sub-volume side are: (a) 11, (b) 21, (c) 25, (d) 42, (e) 62. (For interpretation of the references to color in this figure legend, the reader is referred to the web version of this article.)

likely due to a combination of two separate effects: the smallest sub-volume sizes considered here are comparable with the inner layer thickness, and the fact that for small sub-volumes the discretization (binning) error might be on the same order as the model error (because a small amount of points is actually present in the sub-volume). Additionally, for the methane case two different (linear) error slopes can be clearly distinguished, and a switch between the two is present at the volume size of approximately 1 mm. This is possibly due to the crossing of the flame thermal thickness. In this sense hydrogen presents a rather dissimilar error slope, possibly due to the uneven distribution of mixture fraction (i.e. local equivalence ratio) along the flame given by differential diffusion effects, which leads to a broad

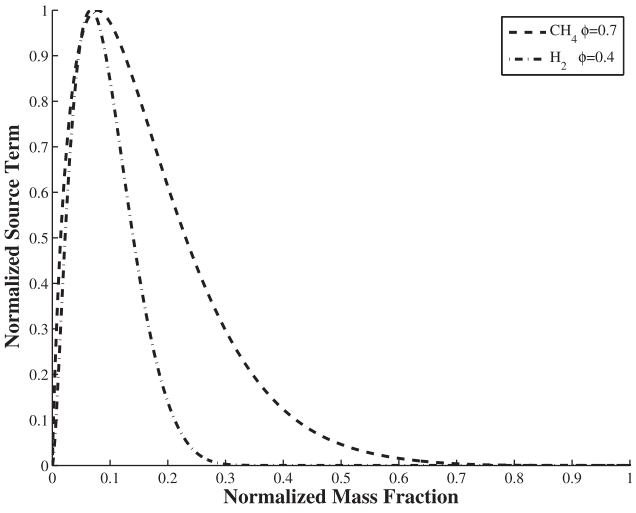

Fig. 9 – Fuel consumption term versus its mass fraction for methane and hydrogen, from 1D premixed flame computations. The conditions adopted for these 1D flames are the same for the 3D computations under analysis in this paper.

spectrum of local flame thicknesses in the domain (in lean premixed hydrogen combustion the flame thickness is extremely sensitive to the equivalence ratio). Fig. 10c displays a direct comparison of the averaged normalized error as a function of the sub-volume size, between the two fuels. This representation shows how the error for the two fuels presents different slopes for equivalent volume size. In addition, it is interesting to notice that for the hydrogen case a decrease of the sub-volume size does not give an appreciable reduction of the error, remarking the lower prediction quality of the presumed β-PDF for hydrogen combustion modeling.

In Section 2 it is explained that the β-function is not able to assume shapes with more than a singular internal peak. To this point, Fig. 11 displays instances of single observations for the hydrogen case in which the β-PDF simply fails (relevant is also the sample of Fig. 4h). This type of β-PDF failures are as a matter of fact rather common among the observations of the hydrogen case, and presumably a source of a large part of the model error.

Summarizing, the *a priori* analysis presented here gives an extended overview of the modeling performance of the presumed β-function, with the peculiarity of a direct confrontation between methane and hydrogen cases. Nonetheless, it

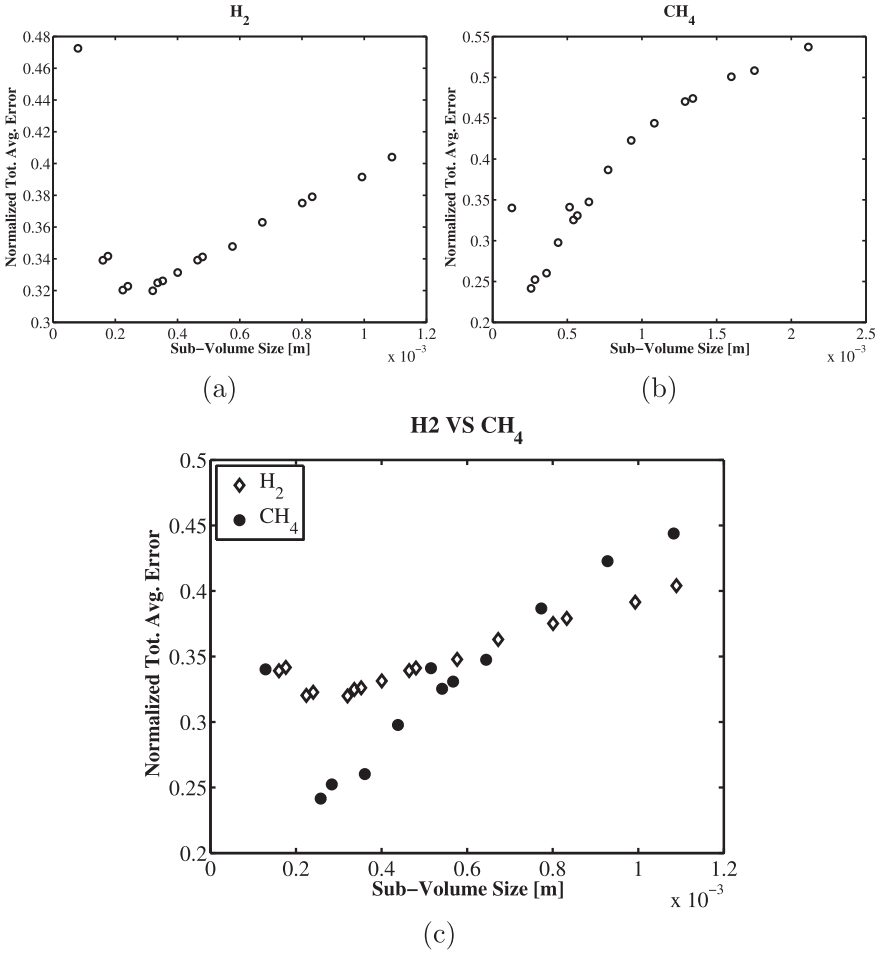

Fig. 10 – Averaged values of the normalized error over the whole domain as a function of the sub-volume size (Δ_{box}). (a) Hydrogen. (b) Methane. (c) Comparison of methane and hydrogen results.

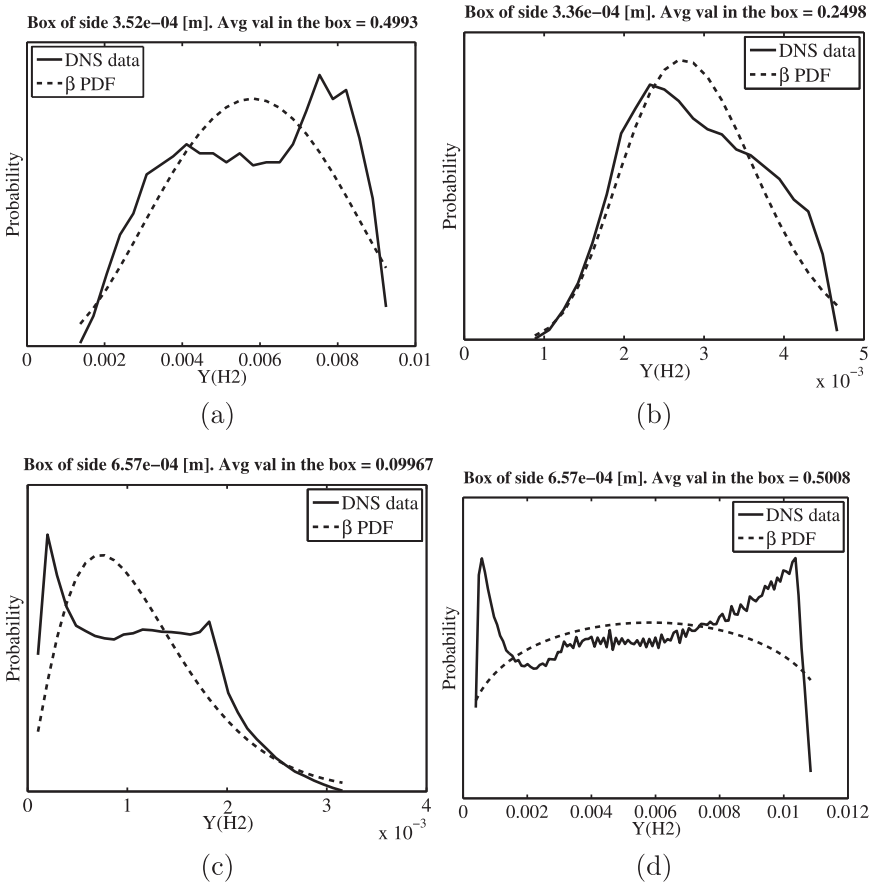

Fig. 11 – Examples of presumed β-PDF failures for hydrogen as a fuel. Comparison of real probability distribution and corresponding β-distribution.

should be carefully kept in mind that the current analysis is not totally exhaustive given that the β-function is evaluated on the local sub-volume extents. In order to complete and improve this investigation, future works should examine the β-function behavior by calculating it considering the overall extents. Such task demands extra care on the choice of the extents, since differential diffusion induces the formation of local super adiabatic values.

A final note must be made in regards to the progress variable definition. In the present paper the progress variable is defined as the fuel mass fraction. Typically, any scalar field can potentially serve as a valid progress variable, with the only restriction of ensuring a monotonic profile of $\mathcal{Y}$ in the whole interval between the unburned mixture and the chemical equilibrium [1,22,23]. This means that the identification of a scalar field that can serve as an unambiguous progress variable is not unique. As a matter of fact, in current combustion models the progress variable is often user defined (based on the experience and intuition). In addition to this, different progress variable definitions lead to different shape of the data in the thermo-chemical space. The behavior of the β-PDF scheme is therefore impacted by how the reaction progress is defined in the present cases. Therefore, it must be noted that the results presented in this paper might be slightly different in the case of a different progress variable choice.

Conclusions

In this paper an investigation of the sub-grid probability density distribution is performed by processing three-dimensional DNS computational results performed with detailed chemistry. This analysis is conducted for hydrogen and methane turbulent flames, with the aim of clarifying the applicability of the β-shaped presumed PDF approach to the modeling of methane and hydrogen turbulent premixed flames. The β-PDF is commonly adopted in combustion because of its capability of modeling Gaussian like distributions as well as a bi-modal behavior which is typical of reacting flows. In particular, it is assessed whether a lean premixed turbulent hydrogen-air flame can be well-represented by a β-PDF approach as traditionally applied for methane in literature. This is done by processing 3D detailed chemistry DNS, for which an *a priori* quantitative comparison between the two distributions is performed in a point to point fashion. The results show that the presumed β-PDF gives a rather good outcome in terms of overall error. Interestingly, it is shown that the total error between the real distribution and the presumed β-PDF is of comparable amount for the two fuels. However, the joint-pdf of the error and progress variable shows a rather defined profile in methane flames (high

probability is distributed on a thin 1D region), whereas for hydrogen the error is more spread throughout a wide region. This leads to the conclusion that the presumed β-PDF model could be improved for methane combustion by empirically adjusting its shape, whereas still keeping the advantage of being simply determined by two parameters (mean and variance). Conversely, it is shown that mean and variance are not sufficient as control parameters for an improved modeling of hydrogen flames by means of presumed PDF, plausibly because of its strong differentially diffusive effects. In addition, it is observed that for both fuels the error of the β-PDF increases for increasing volume size linearly with the sub-volume side length, indicating that the error is locally distributed one-dimensionally.

Acknowledgments

The authors would like to express their gratitude to the Dutch Technology Foundation (STW), Siemens Power Generation and Rolls-Royce Deutschland for the financial support by means of the ALTAS project.

REFERENCES

[1] van Oijen J, de Goey L. Modelling of premixed laminar flames using flamelet-generated manifolds. Combust Sci Technol 2000;161(1):113–37.
[2] Donini A, Bastiaans R, van Oijen J, de Goey L. Differential diffusion effects inclusion with flamelet generated manifold for the modeling of stratified premixed cooled flames. Proc Combust Inst 2014;35(1):831–7.
[3] Fiorina B, Baron R, Gicquel O, Thevenin D, Carpentier S, Darabiha N. Modelling non-adiabatic partially premixed flames using flame-prolongation of ildm. Combust Theory Model 2003;7(3):449–70.
[4] Janicka J, Kollmann W. A two-variables formalism for the treatment of chemical reactions in turbulent H2-air diffusion flames. Proc Combust Inst 1979;17(1):421–30.
[5] Chen M, Herrmann M, Peters N. Flamelet modeling of lifted turbulent methane/air and propane/air jet diffusion flames. Proc Combust Inst 2000;28(1):167–74.
[6] Bray K, Champion M, Libby P, Swaminathan N. Finite rate chemistry and presumed pdf models for premixed turbulent combustion. Combust Flame 2006;146:665–73.
[7] Cook AW, Riley JJ. A subgrid model for equilibrium chemistry in turbulent flows. Phys Fluids 1994;6(8):2868–70.
[8] Vreman A, van Oijen J, Goey L, Bastiaans R. Subgrid scale modeling in large-eddy simulation of turbulent combustion using premixed flamelet chemistry. Flow Turbul Combust 2009;82(4):511–35.
[9] Pitsch H. Large-eddy simulation of turbulent combustion. Annu Rev Fluid Mech 2006;38:453–82.
[10] Donini A, Bastiaans R, van Oijen J, de Goey L. Numerical simulations of a turbulent high-pressure premixed cooled jet flame with the flamelet generated manifolds technique. J Eng Gas Turb Power 2015;137(7). 071501–1/8.
[11] Bondi S, Jones W. A combustion model for premixed flames with varying stoichiometry. Proc Combust Inst 2002;29(2):2123–9.
[12] Bastiaans R, Day M. Analysis of subgrid scale phenomena of premixed turbulent combustion of methane and hydrogen in comparable regimes. Cent Turbul Res Annu Res Briefs 2012:55–66.
[13] Day M, Bell J, Bremer P, Pascucci V, Beckner V, Lijewski M. Turbulence effects on cellular burning structures in lean premixed hydrogen flames. Combust Flame 2009;156:1035–45.
[14] Aspden A, Bell J, Day M. Turbulence-flame interactions in lean premixed hydrogen: transition to the distributed burning regime. J Fluid Mech 2011;680:287–320.
[15] Davis P. Gamma functions and related functions. In: Handbook of mathematical functions. New York: Dover; 1970.
[16] Aspden A, Day M, Bell J. Characterization of low lewis number flames. Proc Combust Inst 2011;33:1463–71.
[17] Day M, Bell J. Numerical simulation of laminar reacting flows with complex chemistry. Combust Theory Model 2000;4:535–56.
[18] Smith G, G. D.M., Frenklach M, Moriarty N, Eiteneer B, Goldenberg M, et al. Gri-Mech 2.11. 1999. URL, http://www.me.berkeley.edu/gri_mech/.
[19] Bell J, Day M. Adaptive methods for simulation of turbulent combustion. Turbul Combust Model 2011;95:301–29.
[20] Chem1D, A one-dimensional laminar flame code, Eindhoven University of Technology. URL http://www.combustion.tue.nl/chem1d.
[21] Donini A, Bastiaans R, van Oijen J, Day M, de Goey L. A priori assessment of the potential of flamelet generated manifolds to model lean turbulent premixed hydrogen combustion. In: Kuerten H, Geurts B, Armenio V, Fröhlich J, editors. Direct and large-Eddy simulation VIII, vol. 15 of ERCOFTAC series. Springer Netherlands; 2011. p. 315–20. URL, http://dx.doi.org/10.1007/978-94-007-2482-2_50.
[22] Poinsot TJ, Veynante DP. Theoretical and numerical combustion, 3/E, T. Poinsot. 2011.
[23] M. Ihme, L. Shunn, J. Zhang, Regularization of reaction progress variable for application to flamelet-based combustion models. J Comput Phys, 231.